

Band gap Engineering by Sublattice Mixing in $\text{Cs}_2\text{AgInCl}_6$: High-throughput Screening from First-principles

Manish Kumar,^{*} Manjari Jain, Arunima Singh, and Saswata Bhattacharya^{*}

Department of Physics, Indian Institute of Technology Delhi, New Delhi, India

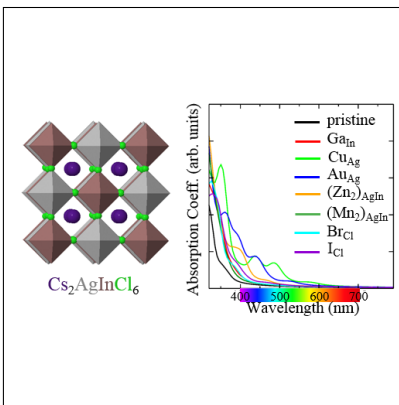
E-mail: manish.kumar@physics.iitd.ac.in[MK]; saswata@physics.iitd.ac.in[SB]

Phone: +91-11-2659 1359. Fax: +91-11-2658 2037

Abstract

Lead-free double perovskite materials (viz. $\text{Cs}_2\text{AgInCl}_6$) are being explored as stable and non-toxic alternatives of lead halide perovskites. In order to expand the optical response of $\text{Cs}_2\text{AgInCl}_6$ in visible region, we report here the stability, electronic structure and optical properties of $\text{Cs}_2\text{AgInCl}_6$ by sublattice mixing of various elements. Here we have employed high-throughput screening using a hierarchical first-principles based approach starting from density functional theory (DFT) with appropriate exchange and correlation functionals to beyond DFT methods under the framework of many body perturbation theory (viz. $\text{G}_0\text{W}_0\text{@HSE06}$). We have started with 32 primary set of combinations of metals M(I), M(II), M(III) and halogen X at Ag/In and Cl site respectively, where concentration of each set is varied to build a database of nearly 140 combinations. The most suitable mixed sublattices are identified to engineer the band gap of $\text{Cs}_2\text{AgInCl}_6$ to have its application in optoelectronic devices under visible light.

Graphical TOC Entry



Keywords

double perovskite, $\text{Cs}_2\text{AgInCl}_6$, defects, hybrid DFT, stability, optical response

Lead halide perovskites APbX_3 ($\text{A} = \text{CH}_3\text{NH}_3^+$, $\text{HC}(\text{NH}_2)_2^+$, Cs^+ , and $\text{X} = \text{Cl}^-$, Br^- , I^-) have created a huge sensation in the field of optoelectronics, particularly photovoltaics owing to their suitable optical band gap, long carrier diffusion length, high carrier mobility and low manufacturing cost.¹⁻⁸ Moreover, the band gap is tunable with high defect tolerance.⁹⁻¹¹ These materials find applications in various optoelectronic devices, namely, solar cells,^{2,12-14} light emitting diodes,^{15,16} lasers^{17,18} and photodetectors.^{19,20} In spite of their great potential in a vast number of applications, there are two major challenges: (i) instability against exposure to humidity, heat or light and (ii) toxicity of Pb. These have posed hindrance in their commercialization. To tackle these issues, many works have been endeavored to find alternative stable and environmentally sustainable metal halide perovskites with fascinating optoelectronic properties akin to lead halide perovskites.²¹⁻²⁵

One of the approaches for removing toxicity is to replace Pb^{2+} with some other divalent metal. However, the replacement using other group divalent cations results in either indirect or large band gap materials with degraded optoelectronic properties.²⁶⁻²⁹ Substitution of group 14 divalent cations, viz. Sn^{2+} and Ge^{2+} have also been synthesized by researchers, but these are not stable at ambient conditions due to the easy oxidation to tetravalent Sn^{4+} and Ge^{4+} , respectively.^{30,31} Another promising approach is to substitute a monovalent $\text{M}(\text{I})$ and a trivalent $\text{M}(\text{III})$ metal alternatively in place of two divalent Pb, that forms the double perovskite $\text{A}_2\text{M}(\text{I})\text{M}(\text{III})\text{X}_6$. Recently, lead-free metal halide double perovskites have been synthesized, which are stable and environmentally benign, viz. $\text{Cs}_2\text{AgBiX}_6$ ($\text{X} = \text{Cl}^-$, Br^- , I^-) and $\text{Cs}_2\text{AgInCl}_6$.³²⁻³⁹ $\text{Cs}_2\text{AgBiX}_6$ perovskites possess indirect band gap, which results in weaker absorption and high non-radiative recombination loss.³²⁻³⁴ In contrast, $\text{Cs}_2\text{AgInCl}_6$ has direct band gap. However, its wide band gap (3.3 eV) does not show optical response in visible region.^{36,37} Alloying with suitable elements could be the best solution to reduce its band gap and expand the spectral response in visible light region.

In this Letter, we have done the sublattice mixing by partial substitution of several metals $\text{M}(\text{I})$, $\text{M}(\text{II})$, $\text{M}(\text{III})$ and halogen X at Ag/In and Cl site, respectively, to reduce the band

gap of $\text{Cs}_2\text{AgInCl}_6$. The idea is to enhance its optical properties for optoelectronic devices. Note that the charge neutrality condition is to be maintained, while the metal/halogen atoms are alloyed by forming substitutional defects. We have performed high-throughput screening by performing hierarchical calculations using first-principles based approaches viz. density functional theory (DFT)^{40,41} with semi-local exchange-correlation (xc) functional (PBE⁴²), hybrid DFT with HSE06⁴³ and single shot GW^{44,45} (G_0W_0) under the many body perturbation theory (MBPT). Firstly, the structural stability analysis has been done by examining the Goldschmidt tolerance factor and octahedral factor. Note that only structural stability is not the sufficient condition to confirm the formation of the perovskites. Therefore, the decomposition enthalpy has been calculated, which reflects the thermodynamic stability of the materials. Further, to get better insights, we have investigated the reduction in band gap via atom projected partial density of states. Finally, by calculating the frequency dependent complex dielectric function, we have determined the optical properties of the materials that can have attractive applications in the field of optoelectronics.

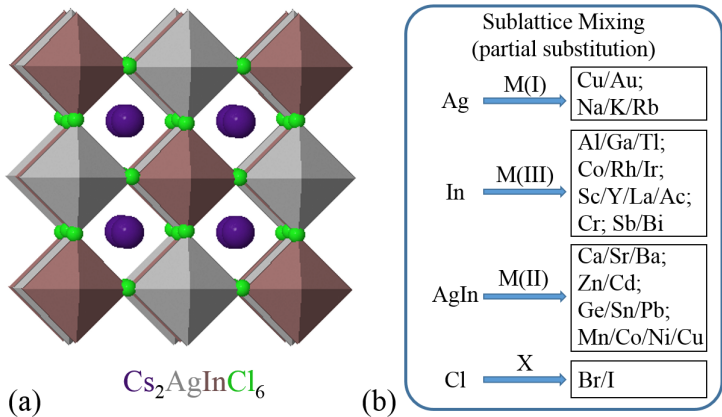


Figure 1: (a) Structure of halide double perovskite $\text{Cs}_2\text{AgInCl}_6$, and (b) Partial substitution with metals M(I), M(II), M(III) and with halogen X at Ag/In and Cl site, respectively, maintaining charge neutrality.

The double perovskite $\text{Cs}_2\text{AgInCl}_6$ has a cubic structure with space group $Fm\bar{3}m$. The corresponding sublattice is composed of alternate octahedra of InCl_6 and AgCl_6 as shown in Figure 1a. On partial substitution of different elements as shown in Figure 1b (metals

and/or halogens), the distortion is very less pronounced. Here we have started with 32 primary set of combinations of metals M(I), M(II), M(III) and halogen X at Ag/In and Cl site respectively, where concentration of each set is varied to build a database of nearly 140 combinations. However, note that here, we have presented the results of 25% substitution for metals and 4% substitution for halogen atoms. This is because we have seen and thoroughly checked that, as we increase the concentration of the external element, if the band gap is increased (or decreased), it increases (or decreases) consistently on further increasing the concentration. Two such test cases are shown in Figure S1 in Supporting Information (SI). We have also reported this, to be the case in our previous experimental finding.⁴⁶ The structural stability of all the alloyed configurations has been determined by calculating two geometrical parameters, viz. the Goldschmidt tolerance factor (t) and the octahedral factor (μ). For single perovskite ABX_3 , $t = (r_A + r_X)/\sqrt{2}(r_B + r_X)$ and $\mu = r_B/r_X$, where r_A , r_B , and r_X are the ionic radii of cation A, B, and anion X, respectively. In case of double perovskites, r_B is the average of the ionic radii at B sites. For stable perovskites, the ranges of t and μ are respectively, $0.8 \leq t \leq 1.0$ and $\mu > 0.41$.⁴⁷ The Shannon ionic radii⁴⁸ have been considered to evaluate t and μ . For the configurations we have considered, t lies between 0.85 and 0.91, and μ has the value between 0.50 and 0.59 (see Table S1). Therefore, these probable structures are stable.

In order to determine the thermodynamic stability, we have computed the decomposition enthalpy (ΔH_D) using PBE and HSE06 xc functionals. We have alloyed the external elements in $Cs_8Ag_4In_4Cl_{24}$ supercell framework to model a solid solution. The ΔH_D for the decomposition of $Cs_8Ag_4In_4Cl_{24}$ into binary compounds is calculated as follows:

$$\Delta H_D(Cs_8Ag_4In_4Cl_{24}) = E(Cs_8Ag_4In_4Cl_{24}) - 8E(CsCl) - 4E(AgCl) - 4E(InCl_3), \quad (1)$$

where $E(Cs_8Ag_4In_4Cl_{24})$, $E(CsCl)$, $E(AgCl)$, and $E(InCl_3)$ are the DFT energies of the respective compounds. The alloyed configurations having negative value of the ΔH_D are

stable. Figure 2a and 2b show the decomposition enthalpy for decomposition of (un)alloyed $\text{Cs}_2\text{AgInCl}_6$ into binary compounds using PBE and HSE06 xc functionals, respectively (decomposition pathways are shown in SI). Only those elements, which lead to decrement in band gap using PBE xc functional, are further considered with HSE06 xc functional. Note that, Tl(III), Cd(II), and Pb(II) are not considered here due to toxicity. The quaternary

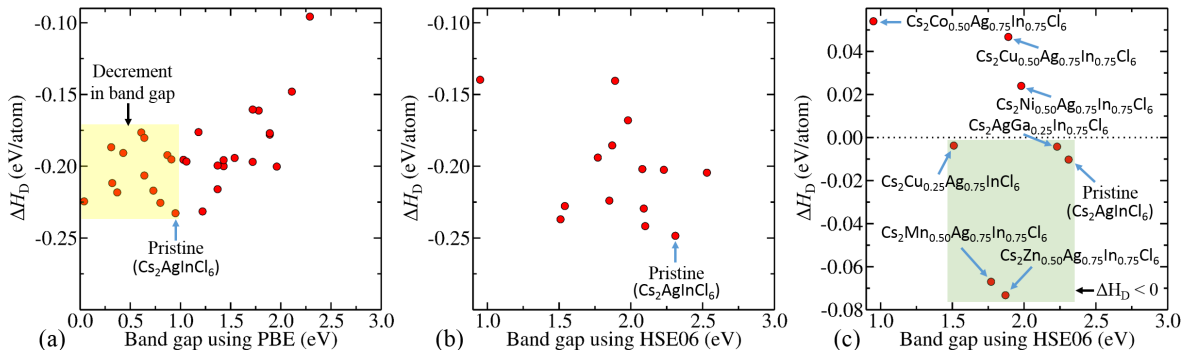


Figure 2: Decomposition enthalpy (ΔH_D) vs band gap for decomposition of pristine and alloyed configurations into binary compounds using the xc functionals (a) PBE and (b) HSE06, and (c) decomposition into ternary compounds using HSE06 xc functional.

compounds can be decomposed into ternary compounds. Therefore, we have also considered those pathways for the materials (see decomposition pathways in SI), which have the favorable band gap. The decomposition enthalpy for decomposition of (un)alloyed $\text{Cs}_2\text{AgInCl}_6$ into ternary compounds is shown in Figure 2c. For decomposition of $\text{Cs}_8\text{Ag}_4\text{In}_4\text{Cl}_{24}$ into ternary compounds, the ΔH_D is determined as follows:

$$\Delta H_D(\text{Cs}_8\text{Ag}_4\text{In}_4\text{Cl}_{24}) = E(\text{Cs}_8\text{Ag}_4\text{In}_4\text{Cl}_{24}) - 2E(\text{CsAgCl}_2) - 2E(\text{Cs}_3\text{In}_2\text{Cl}_9) - 2E(\text{AgCl}). \quad (2)$$

The ΔH_D has the value of -0.248 eV/atom and -0.010 eV/atom for the decomposition of $\text{Cs}_8\text{Ag}_4\text{In}_4\text{Cl}_{24}$ into binary and ternary compounds, respectively. These negative values confirm that the perovskite $\text{Cs}_8\text{Ag}_4\text{In}_4\text{Cl}_{24}$ is stable. We have found that all the selected elements for sublattice mixing are stable with respect to the decomposition into binary compounds (see Table S1). However, for ternary decomposition pathway, Co(II), Ni(II), and Cu(II) are not stable (see Figure 2c). This may be attributed to the smaller size of

these cations that are unable to accommodate two octahedra with Cl_6 . Note that Ni(II) and Cu(II) have the lowest octahedral factor (see Table S1). Also, Cu(I) and Ga(III) are less stable than pristine (see Figure 2c).

A screening of various atoms for sublattice mixing has been done by calculating the band gap first using generalized gradient approximation (PBE). For pristine $\text{Cs}_2\text{AgInCl}_6$, the band gap using PBE xc functional comes out to be 0.95 eV. Further, to see the effect of spin-orbit coupling (SOC) in this material, we have also calculated the band gap using PBE+SOC, which gives a value of 0.93 eV. This implies that SOC has insignificant effect on the electronic properties of $\text{Cs}_2\text{AgInCl}_6$. This corroborates with the fact that it does not contain any heavy element like Pb or Bi, where some significant effect of SOC is expected in the electronic properties of such materials.⁶ Therefore, we have ignored the effect of SOC in our further calculations as the atoms we have considered for substitution are not heavy elements. However, the band gap is highly underestimated by PBE xc functional due to the well known self interaction error. Therefore, we have further performed the calculations using more advanced hybrid xc functional HSE06 for those mixed sublattices, where in comparison to pristine, the band gap was reduced (see Figure 2a, 2b, and Table S1). The calculated value of band gap for $\text{Cs}_2\text{AgInCl}_6$ is 2.31 eV, which is in good agreement with previously reported theoretical value, but still underestimated in comparison to the experimental value (3.3 eV).³⁶ In case of Cu(I) and Au(I) substitutional alloying at Ag site, the band gap is reduced by ~ 0.8 eV, having a value of 1.51 eV and 1.54 eV, respectively. On the other hand, in case of substitution of M(III) at In site, it does not have much effect on reduction in band gap. Only Co(III) and Ir(III) substitutional alloying are able to reduce the band gap from 2.31 eV to 2.08 eV, whereas the rest are either increasing it or have no effect on the band gap. In case of M(II) substitutional alloying, one at Ag and other one at In site, only Zn(II), and Mn(II) are able to reduce the band gap effectively, having a band gap value of 1.87 eV and 1.77 eV, respectively. In case of halogen substitution viz. Br and I, it helps to reduce the band gap to 2.10 and 1.85 eV, respectively (see Table S1).

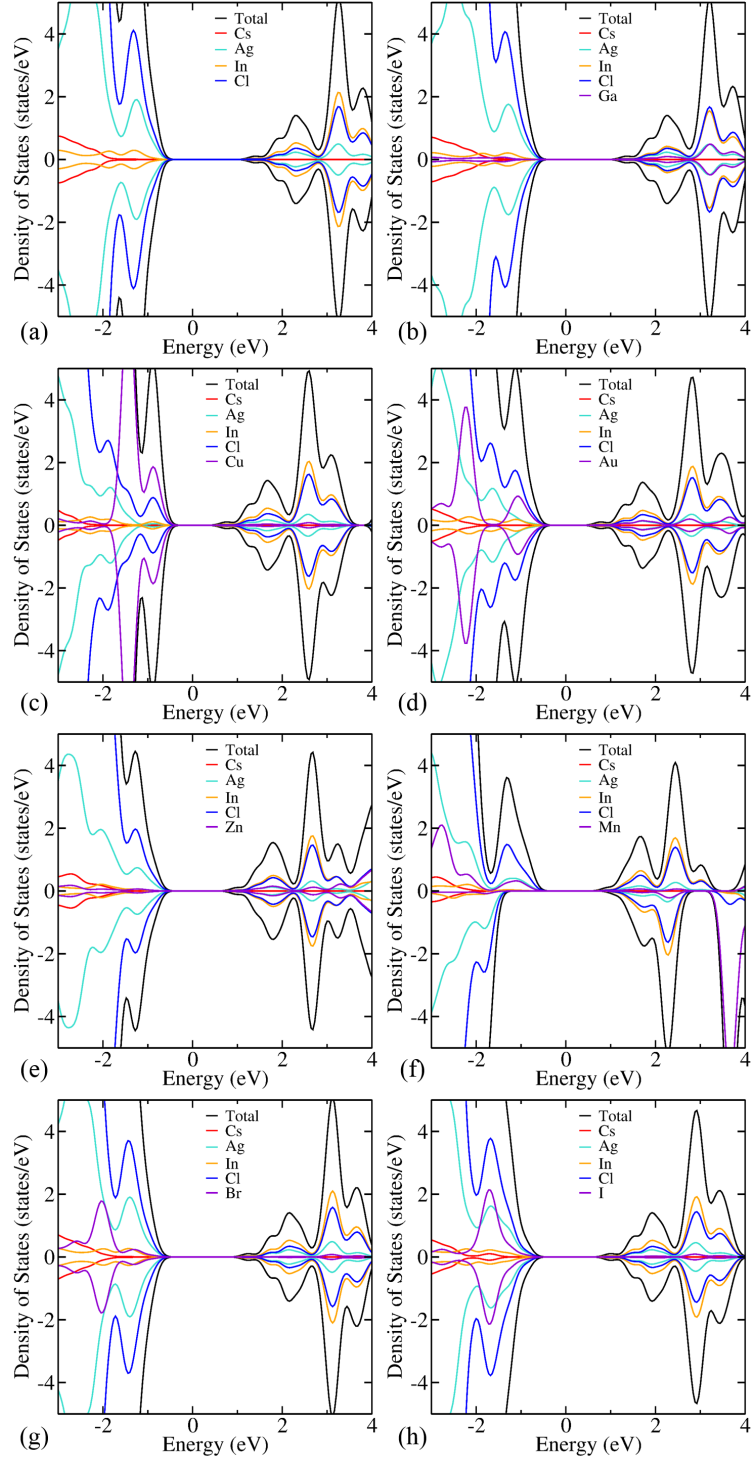


Figure 3: Atom projected partial density of states (pDOS) using HSE06 xc functional of (a) pristine $\text{Cs}_2\text{AgInCl}_6$, (b) $\text{Cs}_2\text{AgGa}_{0.25}\text{In}_{0.75}\text{Cl}_6$, (c) $\text{Cs}_2\text{Cu}_{0.25}\text{Ag}_{0.75}\text{InCl}_6$, (d) $\text{Cs}_2\text{Au}_{0.25}\text{Ag}_{0.75}\text{InCl}_6$, (e) $\text{Cs}_2\text{Zn}_{0.50}\text{Ag}_{0.75}\text{In}_{0.75}\text{Cl}_6$, (f) $\text{Cs}_2\text{Mn}_{0.50}\text{Ag}_{0.75}\text{In}_{0.75}\text{Cl}_6$, (g) $\text{Cs}_2\text{AgInBr}_{0.04}\text{Cl}_{5.96}$, and (h) $\text{Cs}_2\text{AgInI}_{0.04}\text{Cl}_{5.96}$.

The reduction in band gap can be explained by observing the atom projected partial density of states (pDOS) (see Figure 3). In the pristine $\text{Cs}_2\text{AgInCl}_6$, the Cl p-orbitals and Ag d-orbitals contribute to the valence band maximum (VBM), whereas the In and Ag s-orbitals contribute to the conduction band minimum (CBm) (see Figure 3a). The states are symmetric with respect to the spin alignments (spin up or down) indicating that the electrons are paired. In case of substitutional alloying of Cu(I) and Au(I), their d-orbitals have more energy than the Ag d-orbitals and hence, reduce the band gap by elevating the VBM (see Figure 3c and 3d). However, in case of the M(III) substitution at In site, generally, the states lie inside the valence band (VB) or the conduction band (CB), and thus, do not reduce the band gap effectively. From Figure 3b, we can see that the Ga(III) is reducing the band gap by a negligible amount (as the states contributed by the Ga are lying inside VB and CB). Whereas, the Co(III) and Ir(III) substitution at In site show a finite decrease in the band gap. This is due to the Co d-orbitals and Ir d-orbitals contribution at CBm and VBM, respectively (see Figure S2). In case of M(II), there is a little contribution from d- and s-orbitals of M(II) at VBM and CBm, respectively, and therefore, reducing the band gap by introducing the shallow states (see Figure 3e and 3f). The band gap reduction on substituting Br/I at Cl site is occurred by elevating the VBM, which is due to Br/I p-orbitals contribution at VBM (see Figure 3g and 3h). In all these cases, the defect levels are shallow, which is a desirable property for optoelectronic devices. Shallow defect states ensure that the recombination of photogenerated charge carriers is not prominent and thus, the decrement in charge carrier mobility and diffusion will be insignificant.

To obtain the optical properties, that are crucial for the perovskite to be used in optoelectronic devices, we have calculated the frequency dependent complex dielectric function $\epsilon(\omega) = \text{Re}(\epsilon(\omega)) + \text{Im}(\epsilon(\omega))$ using $\text{G}_0\text{W}_0\text{@HSE06}$ (the results with HSE06 xc functional are shown in Figure S3). Figure 4(a) and 4(b) show the imaginary [$\text{Im}(\epsilon)$] and real [$\text{Re}(\epsilon)$] part of the dielectric function, respectively. The real static part (at $\omega = 0$) of the dielectric function is a direct measure of refractive index. Higher the refractive index, better will be

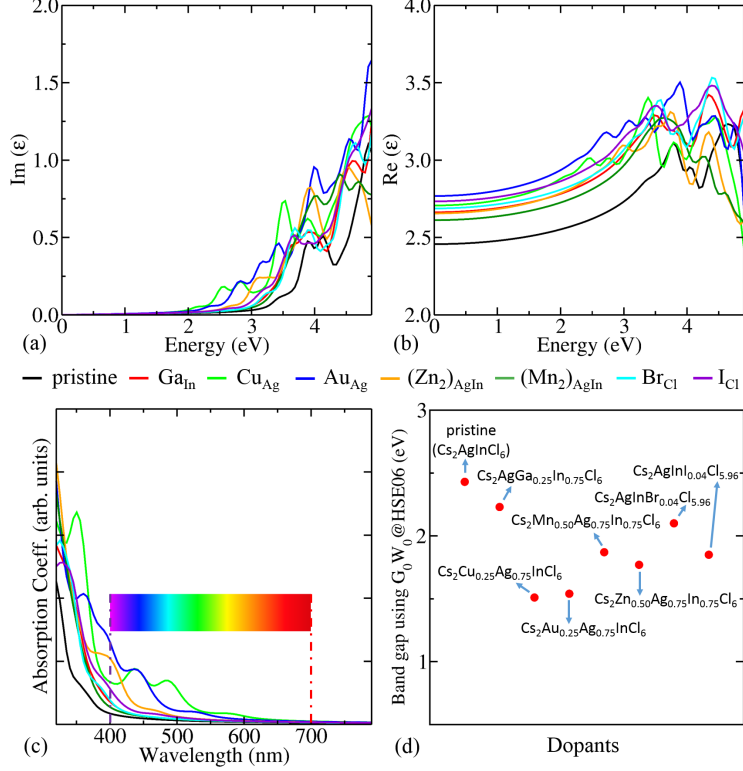


Figure 4: Spatially average (a) imaginary [$\text{Im}(\epsilon)$] and (b) real [$\text{Re}(\epsilon)$] part of the dielectric function, (c) absorption coefficient and (d) band gap obtained by $G_0W_0@HSE06$ for the pristine and alloyed $\text{Cs}_2\text{AgInCl}_6$.

the probability to absorb light. On alloying, the refractive index is increased, and thus, the optical properties are enhanced. Its value is varying from 2.46 – 2.88. The static $\text{Re}(\epsilon)$ is 2.46 for pristine $\text{Cs}_2\text{AgInCl}_6$, and increased on alloying (see Figure 4b, Figure S4 and Table S2). The imaginary part reflects the transitions from occupied to unoccupied bands. The imaginary absorption edge and onset are red shifted and hence, the visible light response is induced on alloying (see Figure 4a). Figure 4c shows the absorption coefficient $\alpha(\omega)$, which is related to real and imaginary part of the dielectric function as follows:

$$\alpha(\omega) = \sqrt{2}\omega \left(\sqrt{\text{Re}(\epsilon(\omega))^2 + \text{Im}(\epsilon(\omega))^2} - \text{Re}(\epsilon(\omega)) \right)^{\frac{1}{2}}. \quad (3)$$

We have seen that on alloying, the peaks of the absorption spectra are red shifted and hence, these mixed sublattices display response in the visible light. This response is attributed to

the reduction in band gap as shown in Figure 4d.

In conclusion, we have investigated the role of metals M(I), M(II), M(III) and halogen X in alloyed $\text{Cs}_2\text{AgInCl}_6$ for inducing the visible light response by tuning its electronic properties for optoelectronic devices using state of the art DFT and beyond DFT methods. We have found that the Goldschmidt tolerance factor and octahedral factor lie in the suitable range to form stable perovskite structure. The decomposition enthalpy of all the mixed sublattices is negative with respect to the binary decomposition indicating that the alloyed systems will not decompose into their binary precursors and thus, are thermodynamically stable. However, Co(II), Ni(II), and Cu(II) are thermodynamically unstable and could decompose into ternary compounds. We have observed that SOC effect is negligible in the double perovskite $\text{Cs}_2\text{AgInCl}_6$ as it does not contain any heavy element like Lead (Pb) and Bismuth (Bi). Many partial substitutional alloying configurations help in reducing the band gap to desired range and thus, increasing the absorption. We have inferred that the sublattices with Cu(I) and Au(I) at Ag site, Co(III) and Ir(III) at In site, Zn(II) at Ag and In site simultaneously, Mn(II) at Ag and In site simultaneously, and Br and I substitution at Cl site as the most promising candidates for various optoelectronic devices.

Computational Methods

The density functional theory (DFT)^{40,41} calculations have been performed using the Vienna *ab initio* simulation package (VASP).^{49,50} The ion-electron interactions in all the elemental constituents are described using projector-augmented wave (PAW) potentials.^{50,51} All the structures are optimized (i.e. the atomic positions are relaxed) using generalized gradient approximation as implemented in PBE⁴² exchange-correlation (xc) functional until the forces are smaller than 0.001 eV/Å. The electronic self consistency loop convergence is set to 0.01 meV, and the kinetic energy cutoff is set to 500 eV for plane wave basis set expansion. A k-point mesh of $4 \times 4 \times 4$ is used for Brillouin zone integration, which is generated using

Monkhorst-Pack⁵² scheme. Advanced hybrid xc functional HSE06⁴³ is used for the better estimation of band gap as well as thermodynamic stability. For determination of the optical properties, single shot GW^{44,45} (G_0W_0) calculations have been performed on top of the orbitals obtained from HSE06 xc functional. The polarizability calculations are carried out on a grid of 50 frequency points. The number of unoccupied bands is set to four times the number of occupied orbitals. Note that spin-orbit coupling (SOC) is not taken into account because it negligibly affects the electronic structure of Ag/In-based halide double perovskite, which is consistent with previous studies.^{53,54}

Acknowledgement

MK acknowledges CSIR, India, for the senior research fellowship [grant no. 09/086(1292)/2017-EMR-I]. MJ acknowledges CSIR, India, for the junior research fellowship [grant no. 09/086(1344)/2018-EMR-I]. AS acknowledges IIT Delhi for the financial support. SB acknowledges the financial support from SERB under core research grant (grant no. CRG/2019/000647). We acknowledge the High Performance Computing (HPC) facility at IIT Delhi for computational resources.

References

- (1) Kojima, A.; Teshima, K.; Shirai, Y.; Miyasaka, T. Organometal Halide Perovskites as Visible-Light Sensitizers for Photovoltaic Cells. *Journal of the American Chemical Society* **2009**, *131*, 6050–6051.
- (2) Lee, M. M.; Teuscher, J.; Miyasaka, T.; Murakami, T. N.; Snaith, H. J. Efficient Hybrid Solar Cells Based on Meso-Superstructured Organometal Halide Perovskites. *Science* **2012**, *338*, 643–647.
- (3) Xing, G.; Mathews, N.; Sun, S.; Lim, S. S.; Lam, Y. M.; Grätzel, M.; Mhaisalkar, S.;

- Sum, T. C. Long-Range Balanced Electron- and Hole-Transport Lengths in Organic-Inorganic CH₃NH₃PbI₃. *Science* **2013**, *342*, 344–347.
- (4) Wehrenfennig, C.; Eperon, G. E.; Johnston, M. B.; Snaith, H. J.; Herz, L. M. High Charge Carrier Mobilities and Lifetimes in Organolead Trihalide Perovskites. *Advanced Materials* **2014**, *26*, 1584–1589.
- (5) Savenije, T. J.; Ponseca, C. S.; Kunneman, L.; Abdellah, M.; Zheng, K.; Tian, Y.; Zhu, Q.; Canton, S. E.; Scheblykin, I. G.; Pullerits, T. et al. Thermally Activated Exciton Dissociation and Recombination Control the Carrier Dynamics in Organometal Halide Perovskite. *The Journal of Physical Chemistry Letters* **2014**, *5*, 2189–2194.
- (6) Basera, P.; Kumar, M.; Saini, S.; Bhattacharya, S. Reducing lead toxicity in the methylammonium lead halide MAPbI₃: Why Sn substitution should be preferred to Pb vacancy for optimum solar cell efficiency. *Phys. Rev. B* **2020**, *101*, 054108.
- (7) Manser, J. S.; Christians, J. A.; Kamat, P. V. Intriguing Optoelectronic Properties of Metal Halide Perovskites. *Chemical Reviews* **2016**, *116*, 12956–13008.
- (8) Swarnkar, A.; Marshall, A. R.; Sanhira, E. M.; Chernomordik, B. D.; Moore, D. T.; Christians, J. A.; Chakrabarti, T.; Luther, J. M. Quantum dot-induced phase stabilization of α -CsPbI₃ perovskite for high-efficiency photovoltaics. *Science* **2016**, *354*, 92–95.
- (9) Steirer, K. X.; Schulz, P.; Teeter, G.; Stevanovic, V.; Yang, M.; Zhu, K.; Berry, J. J. Defect Tolerance in Methylammonium Lead Triiodide Perovskite. *ACS Energy Letters* **2016**, *1*, 360–366.
- (10) Kang, J.; Wang, L.-W. High Defect Tolerance in Lead Halide Perovskite CsPbBr₃. *The Journal of Physical Chemistry Letters* **2017**, *8*, 489–493.

- (11) Tan, H.; Che, F.; Wei, M.; Zhao, Y.; Saidaminov, M. I.; Todorović, P.; Broberg, D.; Walters, G.; Tan, F.; Zhuang, T. et al. Dipolar cations confer defect tolerance in wide-bandgap metal halide perovskites. *Nature communications* **2018**, *9*, 3100.
- (12) Burschka, J.; Pellet, N.; Moon, S.-J.; Humphry-Baker, R.; Gao, P.; Nazeeruddin, M. K.; Grätzel, M. Sequential deposition as a route to high-performance perovskite-sensitized solar cells. *Nature* **2013**, *499*, 316.
- (13) Sanchez, R. S.; Gonzalez-Pedro, V.; Lee, J.-W.; Park, N.-G.; Kang, Y. S.; Mora-Sero, I.; Bisquert, J. Slow Dynamic Processes in Lead Halide Perovskite Solar Cells. Characteristic Times and Hysteresis. *The Journal of Physical Chemistry Letters* **2014**, *5*, 2357–2363.
- (14) Nam, J. K.; Chun, D. H.; Rhee, R. J. K.; Lee, J. H.; Park, J. H. Methodologies toward Efficient and Stable Cesium Lead Halide Perovskite-Based Solar Cells. *Advanced Science* **2018**, *5*, 1800509.
- (15) Li, G.; Tan, Z.-K.; Di, D.; Lai, M. L.; Jiang, L.; Lim, J. H.-W.; Friend, R. H.; Greenham, N. C. Efficient Light-Emitting Diodes Based on Nanocrystalline Perovskite in a Dielectric Polymer Matrix. *Nano Letters* **2015**, *15*, 2640–2644.
- (16) Yantara, N.; Bhaumik, S.; Yan, F.; Sabba, D.; Dewi, H. A.; Mathews, N.; Boix, P. P.; Demir, H. V.; Mhaisalkar, S. Inorganic Halide Perovskites for Efficient Light-Emitting Diodes. *The Journal of Physical Chemistry Letters* **2015**, *6*, 4360–4364.
- (17) Deschler, F.; Price, M.; Pathak, S.; Klintberg, L. E.; Jarausch, D.-D.; Higler, R.; Htner, S.; Leijtens, T.; Stranks, S. D.; Snaith, H. J. et al. High Photoluminescence Efficiency and Optically Pumped Lasing in Solution-Processed Mixed Halide Perovskite Semiconductors. *The Journal of Physical Chemistry Letters* **2014**, *5*, 1421–1426.
- (18) Xing, G.; Mathews, N.; Lim, S. S.; Yantara, N.; Liu, X.; Sabba, D.; Grätzel, M.;

- Mhaisalkar, S.; Sum, T. C. Low-temperature solution-processed wavelength-tunable perovskites for lasing. *Nature materials* **2014**, *13*, 476.
- (19) Li, X.; Yu, D.; Chen, J.; Wang, Y.; Cao, F.; Wei, Y.; Wu, Y.; Wang, L.; Zhu, Y.; Sun, Z. et al. Constructing Fast Carrier Tracks into Flexible Perovskite Photodetectors To Greatly Improve Responsivity. *ACS Nano* **2017**, *11*, 2015–2023, PMID: 28107628.
- (20) Bao, C.; Yang, J.; Bai, S.; Xu, W.; Yan, Z.; Xu, Q.; Liu, J.; Zhang, W.; Gao, F. High Performance and Stable All-Inorganic Metal Halide Perovskite-Based Photodetectors for Optical Communication Applications. *Advanced Materials* **2018**, *30*, 1803422.
- (21) Yin, W.-J.; Yang, J.-H.; Kang, J.; Yan, Y.; Wei, S.-H. Halide perovskite materials for solar cells: a theoretical review. *J. Mater. Chem. A* **2015**, *3*, 8926–8942.
- (22) Saparov, B.; Hong, F.; Sun, J.-P.; Duan, H.-S.; Meng, W.; Cameron, S.; Hill, I. G.; Yan, Y.; Mitzi, D. B. Thin-Film Preparation and Characterization of Cs₃Sb₂I₉: A Lead-Free Layered Perovskite Semiconductor. *Chemistry of Materials* **2015**, *27*, 5622–5632.
- (23) Frolova, L. A.; Anokhin, D. V.; Gerasimov, K. L.; Dremova, N. N.; Troshin, P. A. Exploring the Effects of the Pb²⁺ Substitution in MAPbI₃ on the Photovoltaic Performance of the Hybrid Perovskite Solar Cells. *The Journal of Physical Chemistry Letters* **2016**, *7*, 4353–4357.
- (24) Ganose, A. M.; Savory, C. N.; Scanlon, D. O. Beyond methylammonium lead iodide: prospects for the emergent field of ns² containing solar absorbers. *Chem. Commun.* **2017**, *53*, 20–44.
- (25) Swarnkar, A.; Mir, W. J.; Nag, A. Can B-Site Doping or Alloying Improve Thermal- and Phase-Stability of All-Inorganic CsPbX₃ (X = Cl, Br, I) Perovskites? *ACS Energy Letters* **2018**, *3*, 286–289.

- (26) Filip, M. R.; Giustino, F. Computational Screening of Homovalent Lead Substitution in Organic-Inorganic Halide Perovskites. *The Journal of Physical Chemistry C* **2016**, *120*, 166–173.
- (27) Krbel, S.; Marques, M. A. L.; Botti, S. Stability and electronic properties of new inorganic perovskites from high-throughput ab initio calculations. *J. Mater. Chem. C* **2016**, *4*, 3157–3167.
- (28) Jacobsson, T. J.; Pazoki, M.; Hagfeldt, A.; Edvinsson, T. Goldschmidts Rules and Strontium Replacement in Lead Halogen Perovskite Solar Cells: Theory and Preliminary Experiments on CH₃NH₃SrI₃. *The Journal of Physical Chemistry C* **2015**, *119*, 25673–25683.
- (29) Kumar, A.; Balasubramaniam, K. R.; Kangsabanik, J.; Vikram,; Alam, A. Crystal structure, stability, and optoelectronic properties of the organic-inorganic wide-band-gap perovskite CH₃NH₃BaI₃: Candidate for transparent conductor applications. *Phys. Rev. B* **2016**, *94*, 180105.
- (30) Jellicoe, T. C.; Richter, J. M.; Glass, H. F. J.; Tabachnyk, M.; Brady, R.; Dutton, S. E.; Rao, A.; Friend, R. H.; Credgington, D.; Greenham, N. C. et al. Synthesis and Optical Properties of Lead-Free Cesium Tin Halide Perovskite Nanocrystals. *Journal of the American Chemical Society* **2016**, *138*, 2941–2944.
- (31) Swarnkar, A.; Ravi, V. K.; Nag, A. Beyond Colloidal Cesium Lead Halide Perovskite Nanocrystals: Analogous Metal Halides and Doping. *ACS Energy Letters* **2017**, *2*, 1089–1098.
- (32) Slavney, A. H.; Hu, T.; Lindenberg, A. M.; Karunadasa, H. I. A Bismuth-Halide Double Perovskite with Long Carrier Recombination Lifetime for Photovoltaic Applications. *Journal of the American Chemical Society* **2016**, *138*, 2138–2141.

- (33) McClure, E. T.; Ball, M. R.; Windl, W.; Woodward, P. M. Cs₂AgBiX₆ (X = Br, Cl): New Visible Light Absorbing, Lead-Free Halide Perovskite Semiconductors. *Chemistry of Materials* **2016**, *28*, 1348–1354.
- (34) Volonakis, G.; Filip, M. R.; Haghighirad, A. A.; Sakai, N.; Wenger, B.; Snaith, H. J.; Giustino, F. Lead-Free Halide Double Perovskites via Heterovalent Substitution of Noble Metals. *The Journal of Physical Chemistry Letters* **2016**, *7*, 1254–1259.
- (35) Filip, M. R.; Hillman, S.; Haghighirad, A. A.; Snaith, H. J.; Giustino, F. Band Gaps of the Lead-Free Halide Double Perovskites Cs₂BiAgCl₆ and Cs₂BiAgBr₆ from Theory and Experiment. *The Journal of Physical Chemistry Letters* **2016**, *7*, 2579–2585.
- (36) Volonakis, G.; Haghighirad, A. A.; Milot, R. L.; Sio, W. H.; Filip, M. R.; Wenger, B.; Johnston, M. B.; Herz, L. M.; Snaith, H. J.; Giustino, F. Cs₂InAgCl₆: A New Lead-Free Halide Double Perovskite with Direct Band Gap. *The Journal of Physical Chemistry Letters* **2017**, *8*, 772–778.
- (37) Zhou, J.; Xia, Z.; Molokeev, M. S.; Zhang, X.; Peng, D.; Liu, Q. Composition design, optical gap and stability investigations of lead-free halide double perovskite Cs₂AgInCl₆. *J. Mater. Chem. A* **2017**, *5*, 15031–15037.
- (38) Yang, B.; Chen, J.; Yang, S.; Hong, F.; Sun, L.; Han, P.; Pullerits, T.; Deng, W.; Han, K. Lead-Free Silver-Bismuth Halide Double Perovskite Nanocrystals. *Angewandte Chemie International Edition* **2018**, *57*, 5359–5363.
- (39) Locardi, F.; Cirignano, M.; Baranov, D.; Dang, Z.; Prato, M.; Drago, F.; Ferretti, M.; Pinchetti, V.; Fanciulli, M.; Brovelli, S. et al. Colloidal Synthesis of Double Perovskite Cs₂AgInCl₆ and Mn-Doped Cs₂AgInCl₆ Nanocrystals. *Journal of the American Chemical Society* **2018**, *140*, 12989–12995.
- (40) Hohenberg, P.; Kohn, W. Inhomogeneous Electron Gas. *Phys. Rev.* **1964**, *136*, B864–B871.

- (41) Kohn, W.; Sham, L. J. Self-Consistent Equations Including Exchange and Correlation Effects. *Phys. Rev.* **1965**, *140*, A1133–A1138.
- (42) Perdew, J. P.; Burke, K.; Ernzerhof, M. Generalized Gradient Approximation Made Simple. *Phys. Rev. Lett.* **1996**, *77*, 3865–3868.
- (43) Krukau, A. V.; Vydrov, O. A.; Izmaylov, A. F.; Scuseria, G. E. Influence of the exchange screening parameter on the performance of screened hybrid functionals. *The Journal of Chemical Physics* **2006**, *125*, 224106.
- (44) Hedin, L. New Method for Calculating the One-Particle Green’s Function with Application to the Electron-Gas Problem. *Phys. Rev.* **1965**, *139*, A796–A823.
- (45) Hybertsen, M. S.; Louie, S. G. First-Principles Theory of Quasiparticles: Calculation of Band Gaps in Semiconductors and Insulators. *Phys. Rev. Lett.* **1985**, *55*, 1418–1421.
- (46) Lamba, R. S.; Basera, P.; Bhattacharya, S.; Sapra, S. Band Gap Engineering in Cs₂(Na_xAg_{1-x})BiCl₆ Double Perovskite Nanocrystals. *The Journal of Physical Chemistry Letters* **2019**, *10*, 5173–5181.
- (47) Travis, W.; Glover, E. N. K.; Bronstein, H.; Scanlon, D. O.; Palgrave, R. G. On the application of the tolerance factor to inorganic and hybrid halide perovskites: a revised system. *Chem. Sci.* **2016**, *7*, 4548–4556.
- (48) Shannon, R. D. Revised effective ionic radii and systematic studies of interatomic distances in halides and chalcogenides. *Acta Crystallographica Section A* **1976**, *32*, 751–767.
- (49) Kresse, G.; Furthmüller, J. Efficiency of ab-initio total energy calculations for metals and semiconductors using a plane-wave basis set. *Computational Materials Science* **1996**, *6*, 15 – 50.

- (50) Kresse, G.; Joubert, D. From ultrasoft pseudopotentials to the projector augmented-wave method. *Phys. Rev. B* **1999**, *59*, 1758–1775.
- (51) Blöchl, P. E. Projector augmented-wave method. *Phys. Rev. B* **1994**, *50*, 17953–17979.
- (52) Monkhorst, H. J.; Pack, J. D. Special points for Brillouin-zone integrations. *Phys. Rev. B* **1976**, *13*, 5188–5192.
- (53) Tran, T. T.; Panella, J. R.; Chamorro, J. R.; Morey, J. R.; McQueen, T. M. Designing indirect-direct bandgap transitions in double perovskites. *Mater. Horiz.* **2017**, *4*, 688–693.
- (54) Cai, Y.; Xie, W.; Teng, Y. T.; Harikesh, P. C.; Ghosh, B.; Huck, P.; Persson, K. A.; Mathews, N.; Mhaisalkar, S. G.; Sherburne, M. et al. High-throughput Computational Study of Halide Double Perovskite Inorganic Compounds. *Chemistry of Materials* **2019**, *31*, 5392–5401.

Band gap engineering by sublattice mixing in $\text{Cs}_2\text{AgInCl}_6$: High-throughput screening from first-principles

Manish Kumar,^{*} Manjari Jain, Arunima Singh, and Saswata Bhattacharya^{*}

Department of Physics, Indian Institute of Technology Delhi, New Delhi, India

E-mail: manish.kumar@physics.iitd.ac.in[MK]; saswata@physics.iitd.ac.in[SB]

Phone: +91-11-2659 1359. Fax: +91-11-2658 2037

Supplemental Material

- I. Change in band gap on increasing concentration of the dopants
- II. Tolerance factor, octahedral factor, band gap and decomposition enthalpy (decomposition into binary compounds) using PBE and HSE06 xc functional of (un)doped $\text{Cs}_2\text{AgInCl}_6$
- III. Reactions for decomposition of pristine and doped $\text{Cs}_2\text{AgInCl}_6$ into binary/ternary compounds
- IV. Density of states of $\text{Cs}_2\text{AgCo}_{0.25}\text{In}_{0.75}\text{Cl}_6$ and $\text{Cs}_2\text{AgIr}_{0.25}\text{In}_{0.75}\text{Cl}_6$
- V. Optical properties of (un)doped $\text{Cs}_2\text{AgInCl}_6$ using HSE06 xc functional
- VI. Optical properties of $\text{Cs}_2\text{AgCo}_{0.25}\text{In}_{0.75}\text{Cl}_6$ and $\text{Cs}_2\text{AgIr}_{0.25}\text{In}_{0.75}\text{Cl}_6$ using $\text{G}_0\text{W}_0@\text{HSE06}$
- VII. Dielectric constant (ϵ_∞) of un(doped) $\text{Cs}_2\text{AgInCl}_6$ using $\text{G}_0\text{W}_0@\text{HSE06}$

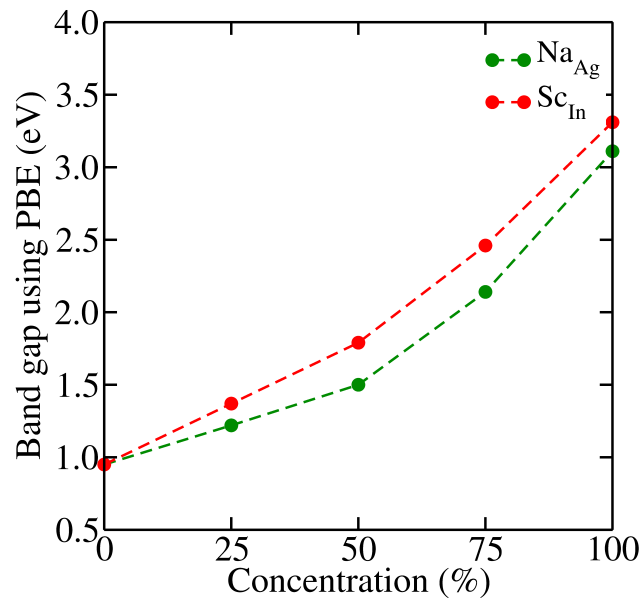
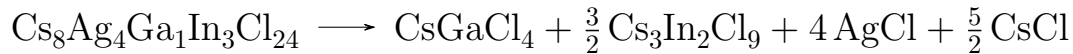
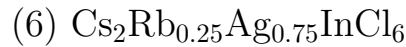
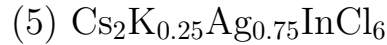
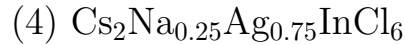
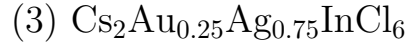
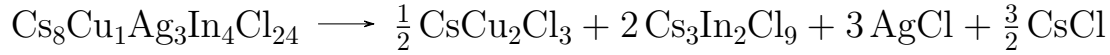
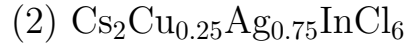


Figure S1: Change in band gap on increasing concentration of the impurity atoms.

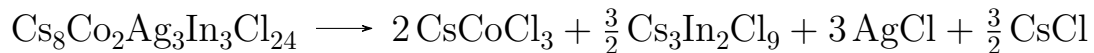
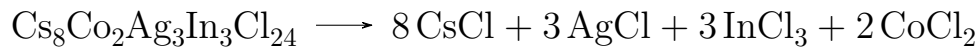
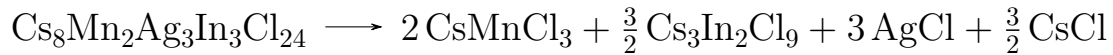
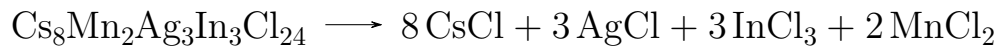
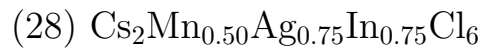
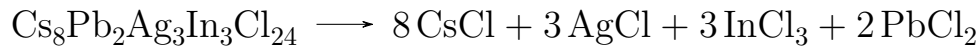
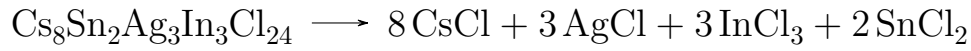
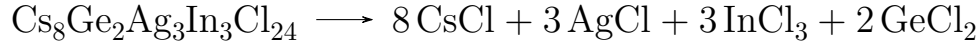
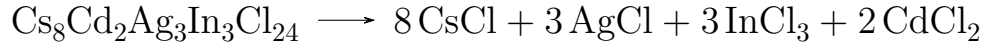
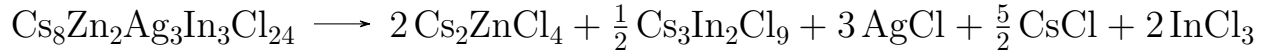
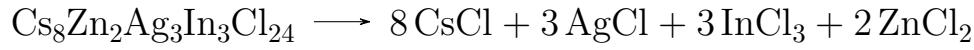
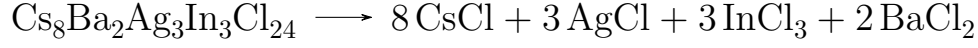
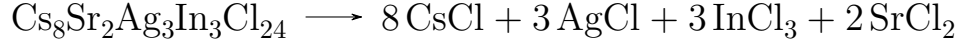
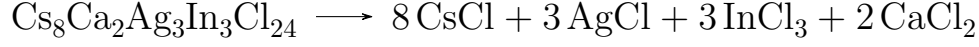
Table S1: Tolerance factor, octahedral factor, band gap and decomposition enthalpy (decomposition into binary compounds) using PBE and HSE06 xc functional of different configurations

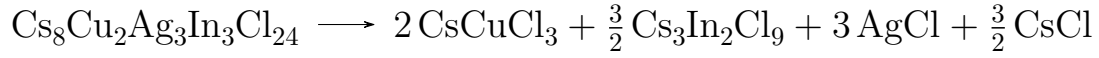
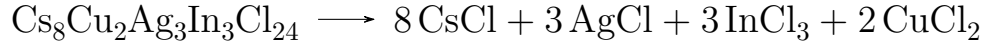
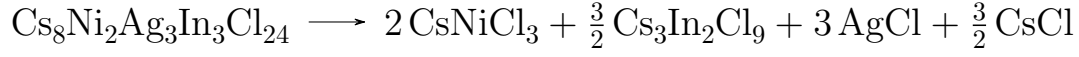
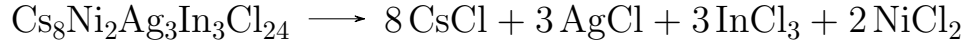
| Configuration | Tolerance factor (t) | Octahedral factor (μ) | Band gap (PBE) (eV) | ΔH_D (binary decomposition) (PBE) (eV/atom) | Band gap HSE06 (eV) | ΔH_D (binary decomposition) (HSE06) (eV/atom) |
|--|--------------------------|-----------------------------|---------------------|---|---------------------|---|
| Cs ₂ AgInCl ₆ | 0.88 | 0.54 | 0.95 | -0.233 | 2.31 | -0.248 |
| Cs ₂ Cu _{0.25} Ag _{0.75} InCl ₆ | 0.90 | 0.51 | 0.04 | -0.224 | 1.51 | -0.237 |
| Cs ₂ Au _{0.25} Ag _{0.75} InCl ₆ | 0.87 | 0.55 | 0.32 | -0.212 | 1.54 | -0.228 |
| Cs ₂ Na _{0.25} Ag _{0.75} InCl ₆ | 0.89 | 0.53 | 1.22 | -0.232 | | |
| Cs ₂ K _{0.25} Ag _{0.75} InCl ₆ | 0.87 | 0.55 | 1.37 | -0.216 | | |
| Cs ₂ Rb _{0.25} Ag _{0.75} InCl ₆ | 0.87 | 0.56 | 1.43 | -0.200 | | |
| Cs ₂ AgAl _{0.25} In _{0.75} Cl ₆ | 0.89 | 0.52 | 1.03 | -0.196 | | |
| Cs ₂ AgGa _{0.25} In _{0.75} Cl ₆ | 0.89 | 0.53 | 0.87 | -0.192 | 2.23 | -0.202 |
| Cs ₂ AgTl _{0.25} In _{0.75} Cl ₆ | 0.88 | 0.54 | 0.37 | -0.218 | | |
| Cs ₂ AgCo _{0.25} In _{0.75} Cl ₆ | 0.89 | 0.52 | 0.73 | -0.217 | 2.09 | -0.230 |
| Cs ₂ AgRh _{0.25} In _{0.75} Cl ₆ | 0.89 | 0.53 | 0.91 | -0.195 | 2.53 | -0.204 |
| Cs ₂ AgIr _{0.25} In _{0.75} Cl ₆ | 0.89 | 0.53 | 0.43 | -0.191 | 2.08 | -0.202 |
| Cs ₂ AgSc _{0.25} In _{0.75} Cl ₆ | 0.89 | 0.53 | 1.37 | -0.200 | | |
| Cs ₂ AgY _{0.25} In _{0.75} Cl ₆ | 0.88 | 0.54 | 1.54 | -0.194 | | |
| Cs ₂ AgLa _{0.25} In _{0.75} Cl ₆ | 0.87 | 0.55 | 1.89 | -0.178 | | |
| Cs ₂ AgAc _{0.25} In _{0.75} Cl ₆ | 0.87 | 0.56 | 1.78 | -0.161 | | |
| Cs ₂ AgCr _{0.25} In _{0.75} Cl ₆ | 0.89 | 0.53 | 1.06 | -0.197 | | |
| Cs ₂ AgSb _{0.25} In _{0.75} Cl ₆ | 0.89 | 0.54 | 1.72 | -0.197 | | |
| Cs ₂ AgBi _{0.25} In _{0.75} Cl ₆ | 0.87 | 0.55 | 1.96 | -0.200 | | |
| Cs ₂ Ca _{0.50} Ag _{0.75} In _{0.75} Cl ₆ | 0.88 | 0.54 | 1.89 | -0.177 | | |
| Cs ₂ Sr _{0.50} Ag _{0.75} In _{0.75} Cl ₆ | 0.87 | 0.57 | 2.11 | -0.148 | | |
| Cs ₂ Ba _{0.50} Ag _{0.75} In _{0.75} Cl ₆ | 0.85 | 0.59 | 2.29 | -0.096 | | |
| Cs ₂ Zn _{0.50} Ag _{0.75} In _{0.75} Cl ₆ | 0.90 | 0.51 | 0.61 | -0.176 | 1.87 | -0.186 |
| Cs ₂ Cd _{0.50} Ag _{0.75} In _{0.75} Cl ₆ | 0.89 | 0.54 | 0.64 | -0.180 | | |
| Cs ₂ Ge _{0.50} Ag _{0.75} In _{0.75} Cl ₆ | 0.90 | 0.50 | 1.43 | -0.196 | | |
| Cs ₂ Sn _{0.50} Ag _{0.75} In _{0.75} Cl ₆ | 0.87 | 0.57 | 1.18 | -0.176 | | |
| Cs ₂ Pb _{0.50} Ag _{0.75} In _{0.75} Cl ₆ | 0.87 | 0.57 | 1.72 | -0.160 | | |
| Cs ₂ Mn _{0.50} Ag _{0.75} In _{0.75} Cl ₆ | 0.90 | 0.52 | 0.31 | -0.187 | 1.77 | -0.194 |
| Cs ₂ Co _{0.50} Ag _{0.75} In _{0.75} Cl ₆ | 0.90 | 0.51 | metallic | -0.166 | 0.95 | -0.140 |
| Cs ₂ Ni _{0.50} Ag _{0.75} In _{0.75} Cl ₆ | 0.91 | 0.50 | metallic | -0.160 | 1.98 | -0.168 |
| Cs ₂ Cu _{0.50} Ag _{0.75} In _{0.75} Cl ₆ | 0.90 | 0.50 | metallic | -0.172 | 1.89 | -0.140 |
| Cs ₂ AgInBr _{0.04} Cl _{5.96} | 0.88 | 0.54 | 0.80 | -0.226 | 2.10 | -0.242 |
| Cs ₂ AgInI _{0.04} Cl _{5.96} | 0.88 | 0.54 | 0.64 | -0.206 | 1.85 | -0.224 |

Reactions for decomposition of pristine and doped $\text{Cs}_2\text{AgInCl}_6$ into binary/ternary compounds:









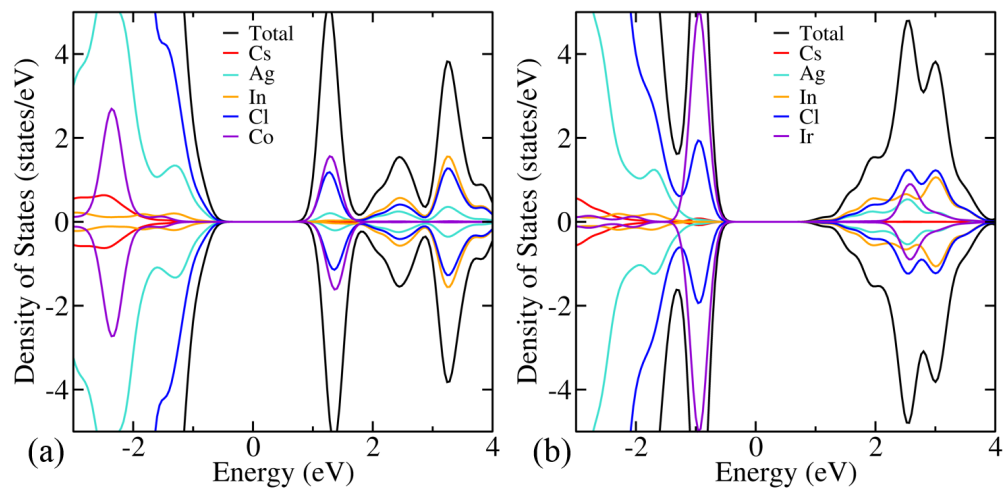


Figure S2: Atom projected partial density of states (pDOS) using HSE06 xc functional of (a) $\text{Cs}_2\text{AgCo}_{0.25}\text{In}_{0.75}\text{Cl}_6$ and (b) $\text{Cs}_2\text{AgIr}_{0.25}\text{In}_{0.75}\text{Cl}_6$.

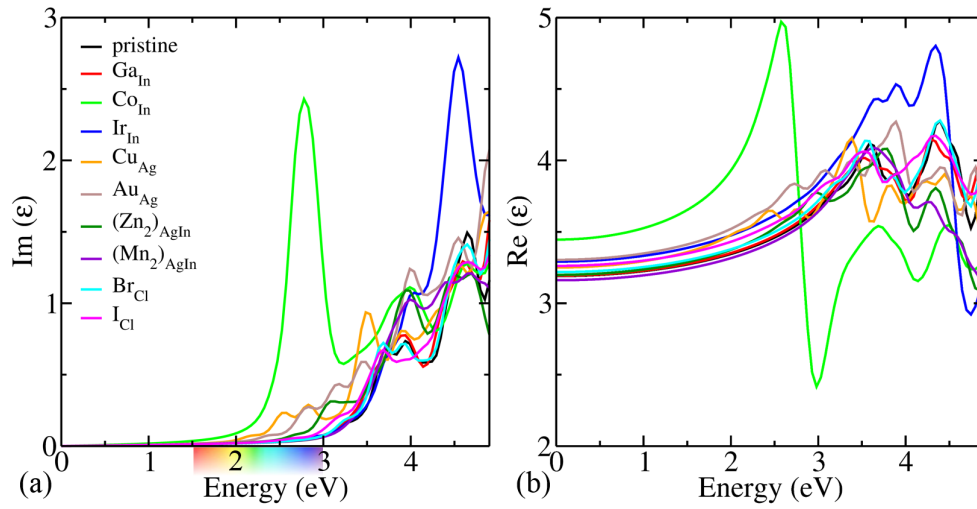


Figure S3: Spatially average (a) imaginary $[\text{Im}(\epsilon)]$ and (b) real $[\text{Re}(\epsilon)]$ part of the dielectric function obtained by HSE06 for the pristine, and doped $\text{Cs}_2\text{AgInCl}_6$.

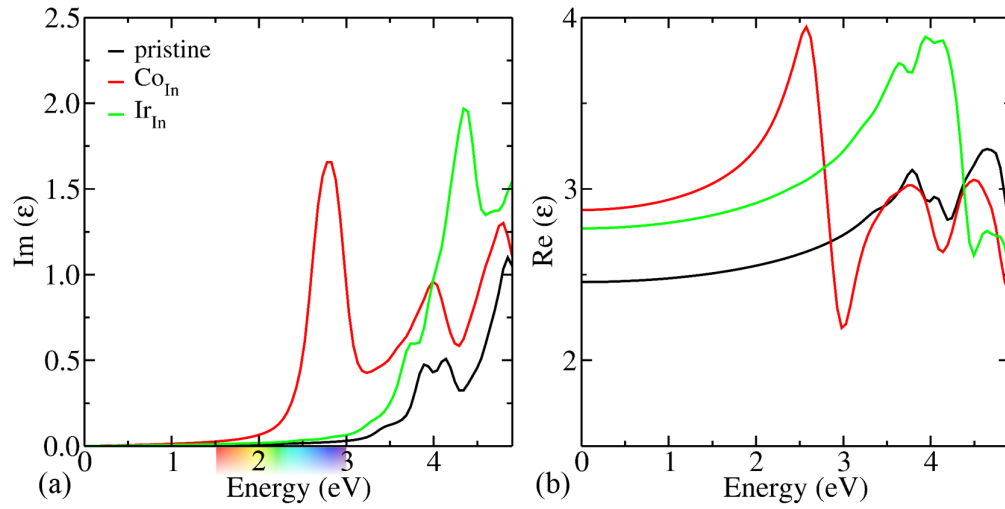


Figure S4: Spatially average (a) imaginary [$\text{Im}(\epsilon)$] and (b) real [$\text{Re}(\epsilon)$] part of the dielectric function obtained by $G_0W_0@HSE06$ for the pristine, $\text{Cs}_2\text{AgCo}_{0.25}\text{In}_{0.75}\text{Cl}_6$, and $\text{Cs}_2\text{AgIr}_{0.25}\text{In}_{0.75}\text{Cl}_6$.

Table S2: The high frequency ‘ion-clamped’ dielectric constant (ϵ_∞) using $G_0W_0@HSE06$

| Configurations | ϵ_∞ |
|--|-------------------|
| pristine | 2.46 |
| $\text{Cs}_2\text{AgGa}_{0.25}\text{In}_{0.75}\text{Cl}_6$ | 2.66 |
| $\text{Cs}_2\text{AgCo}_{0.25}\text{In}_{0.75}\text{Cl}_6$ | 2.88 |
| $\text{Cs}_2\text{AgIr}_{0.25}\text{In}_{0.75}\text{Cl}_6$ | 2.77 |
| $\text{Cs}_2\text{Cu}_{0.25}\text{Ag}_{0.75}\text{InCl}_6$ | 2.71 |
| $\text{Cs}_2\text{Au}_{0.25}\text{Ag}_{0.75}\text{InCl}_6$ | 2.77 |
| $\text{Cs}_2\text{Zn}_{0.50}\text{Ag}_{0.75}\text{In}_{0.75}\text{Cl}_6$ | 2.66 |
| $\text{Cs}_2\text{Mn}_{0.50}\text{Ag}_{0.75}\text{In}_{0.75}\text{Cl}_6$ | 2.61 |
| $\text{Cs}_2\text{AgInBr}_{0.04}\text{Cl}_{5.96}$ | 2.69 |
| $\text{Cs}_2\text{AgInI}_{0.04}\text{Cl}_{5.96}$ | 2.73 |